International Journal of Materials Science and Applications
2014; 3(2): 29-36
Published online February 28, 2014 (http://www.sciencepublishinggroup.com/j/ijmsa)
doi: 10.11648/j.ijmsa.20140302.14

Sputter rate distribution and compositional variations in films sputtered from elemental and multi-element targets at different pressures

Erik Särhammar[1, *], Erik Strandberg[1], Nicolas Martin[2], Tomas Nyberg[1]

[1]Department of Solid State Electronics, Uppsala University, Uppsala, Sweden
[2]Micro Nano Sciences & Systems Department, Institute FEMTO-ST, Université de Franche-Comté, France

Email address:
erik.sarhammar@angstrom.uu.se (E. Särhammar)

To cite this article:
Erik Särhammar, Erik Strandberg, Nicolas Martin, Tomas Nyberg. Sputter Rate Distribution and Compositional Variations in Films Sputtered from Elemental and Multi-Element Targets at Different Pressures. *International Journal of Materials Science and Applications*. Vol. 3, No. 2, 2014, pp. 29-36. doi: 10.11648/j.ijmsa.20140302.14

Abstract: We report on the quantitative dependence of the deposition rate during magnetron sputtering as a function of the atomic mass, processing pressure and substrate location relative to the target. Targets made of four different materials (C, Al, Ti and Ta), ranging from very light to rather heavy atomic masses, were investigated theoretically initially to determine the deposition rate distribution of the sputtered atoms. In the second part, targets made of different combinations of these materials (Ta/C, Ta/Al, Ta/Ti and Ti/Al) were sputtered to investigate the compositional variations of deposited films. The different targets were sputtered at both low (0.27 Pa) and high (2.7 Pa) pressures, and both the deposition rates and compositions were determined at four different locations in the chamber. Further, Monte Carlo simulations were performed for the sputtered atoms in a simplified model of the vacuum chamber. Simulation and experiments are in adequate agreement and show a significant influence of the processing pressure on the deposition rate in various locations of the chamber. This effect is different for different target compositions and may sometimes result in very large compositional variations in films sputtered from segmented multi-element or alloy targets. Transport phenomena of the sputtered particles are also discussed based on a ballistic or diffusion-like process, depending on the sputtering pressure, mass and size of the sputtered atom as well as location in the deposition chamber. Since the materials studied range from light to heavy and the processing pressures cover the values where sputtering normally takes place, the results in this work can be extrapolated to predict the deposition profiles and compositional gradients for arbitrary material combinations and processing pressures.

Keywords: Magnetron Sputtering, Deposition Rate Distribution, Monte Carlo Simulations, Gas Scattering

1. Introduction

In conventional sputtering, the substrate is commonly placed right in front of the target to enable a high deposition rate and low loss of target material. In an ideal process, all sputtered atoms end up at the substrate and nothing on the chamber walls. However, in reality the loss of material may be significant and is dependent on a number of parameters, such as processing pressure, atomic weight and the angular distribution of sputtered particles as well as the position of the substrate relative to the target [1-5]. Given a certain target material, the only parameters that may be changed to influence the process are pressure and substrate position. If the pressure is increased, the sputtered atoms will scatter more frequently resulting in a more diffusion like transport process. These are well-known effects, which have been qualitatively studied [6-12] but few works report on their quantitative aspects [13-18].

It is also well known that the processing pressure and chamber geometry have a significant impact on the deposition profile and film properties of the sputtering process. Surfaces in “line of sight” of the target normally exhibit a higher deposition rate and a higher flux of energetic particles resulting in a thicker more compact and crystalline film [19]. This is, however, mostly true for sputtering at low pressures, where the mean free path is relatively large and collisions are rare. Here, most of the atoms reach the substrate after none, or just a few, collisions, maintaining a large portion of their initial energy. Increasing the pressure leads to a reduction of the mean free path and more frequent collisions, resulting in a loss of energy and increased

scattering. Further, scattering is strongly dependent on the mass of the sputtered species. On average, small and light atoms (with respect to Ar) tend to have large scattering angles, sometimes 180 degrees, while heavy atoms do not deflect significantly from their path. Consequently, heavier atoms need several collisions to make a U-turn and come back to the target and surrounding areas, while lighter atoms may only need one collision.

The species dependent scattering behaviour may result in significant compositional gradients when sputtering from compound targets. Sputtering from such targets is widely used for deposition of multi-element complex compound films where the compositions are potentially vital for their properties. To understand and predict such compositional variations, it is desirable to model the mechanisms responsible for these gradients.

In this work, the transport of sputtered particles to the substrate/chamber wall is studied both experimentally as well as by Monte Carlo simulations. It should be pointed out that this study is limited to the sputtered flux distribution over the chamber and does not include the final energy or angle of the sputtered atoms upon deposition. In a first study, four different materials (C, Al, Ti and Ta) were sputtered at two different pressures (0.27 Pa and 2.7 Pa) and the deposition rates were measured at four different positions (I to IV) in the chamber, Fig. 1. In a second study, the targets were cut in pieces and mounted in different combinations (Ta/C, Ta/Al, Ta/Ti and Ti/Al) and were sputtered to investigate the compositional variations of deposited films at the same positions and pressures. The results were compared with Monte Carlo simulations. The materials and processing pressures were selected to cover a wide range of processing conditions so that the results presented here may be used to predict the deposition profile and compositional gradients for arbitrary materials at any sputtering pressure.

2. Experimental Details

Experiments were performed in a cryo-pumped home-built stainless steel vacuum chamber with cylindrical dimensions (height 0.3 m x diameter 0.3 m). In the first part of the study, depositions were carried out at two different pressures (0.27 Pa and 2.7 Pa) by DC magnetron sputtering from C, Al, Ti and Ta targets. In the second part, the targets were separated into two equally sized pieces and mounted on the magnetron which enabled sputtering from Ta/C, Ta/Al, Ta/Ti and Ti/Al targets. Each target was 2 inch in diameter and mounted on a Lesker magnetron. A constant power of 60W was applied by an ENI DC power supply, resulting in target voltages in the range of 300-400V depending on target material and processing pressure. The base pressure (<$2x10^{-4}$ Pa) was measured with a hot cathode ionization gauge, while the processing pressure was measured with a capacitance gauge. The Ar flow was set to 4 sccm and 47 sccm in order to get 0.27 Pa and 2.7 Pa sputtering pressures respectively, resulting in an effective pumping speed of 28 and 33 L/s, respectively. Si substrates were located at four different positions, I to IV, in the vacuum chamber (Fig. 1). The distance from the centre of the target to the substrate is: position I – 20 cm, position II – 18 cm, position III – 14 cm and position IV – 5 cm.

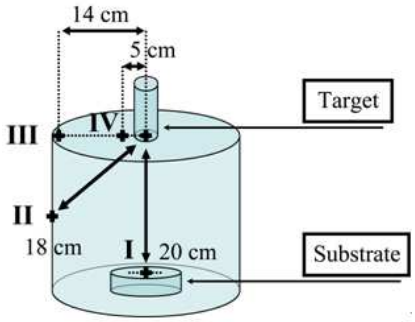

Figure 1. *Schematic view of the vacuum chamber. I, II, III and IV represents the different positions of the substrates. All positions and the centre of the target are coplanar. Distances between the centre of the target and the positions are indicated. Sample I is mounted in front of the target. Sample II is mounted halfway on the wall. Samples III and IV are aligned with the target.*

Four films were simultaneously deposited onto small test substrates at positions I to IV in the chamber for each material at the two different pressures. The substrates were placed along the projected line of symmetry defining the cut between the two target pieces when multi-element targets were used. The counts/signal from each material obtained by Energy-dispersive X-ray spectroscopy (EDS) (Zeiss LEO 440 with a LaB6 crystal) was used as a relative measurement of the deposition rate (i.e. number of atoms per unit area). The accelerating voltage was chosen high enough to get a significant signal from the Si substrate. This procedure was used in order to ensure a correlation between the number of atoms per unit area in the film and the EDS intensity from the material. The EDS was combined with X-ray photoelectron spectroscopy (XPS) (PHI Quantum 2000 with Al K_α radiation source) to obtain the composition of the films deposited from multi-element targets.

3. Simulations

A simulation program was developed to gain a better understanding of the sputtering process. The Monte Carlo program is used to simulate more than $5x10^7$ individual particles at a time. For each particle the simulation consists of the following main steps. First, the particle is given an initial position on the target from which it is to be sputtered. A uniform approximation of a race-track (30-70% of the target radius) is assumed and the particle's position is randomly selected. Next, the particle is given an initial direction and energy. This is done by using SRIM [20] (with 400 eV Ar^+ ions), which yields a distribution of ejected atoms with their corresponding take-off direction and initial energy. This is a rather idealized picture assuming a completely flat target surface. In reality, the target has a certain surface roughness that will influence the take-off

angle. The output data from SRIM is used to generate the initial direction and energy for the sputtered particle. Finally, the program follows each particle on its way through the chamber. This is carried out according to the following procedure:

1. Determine how far the particle will travel before its next collision. This is done by randomly generating the length *l*, using the particles mean free path.
2. Calculate the new position P_1, given the length *l*, the direction, and the initial position P_0.
3. Determine if the particle would hit any surface when moving from point P_0 to point P_1. If so, calculate the particle's energy and direction upon the impact with the surface and start simulating a new particle.
4. Assume that the particle collides with an Ar atom. Randomly generate the impact parameter *r* between the two colliding particles. Here, the motion of the Ar atom is taken into account. Calculate the angular scattering that the particles will undergo as well as their energy after the collision. The azimuthal angle is now randomly selected from the interval [0, 2π]. From this, the particle's new direction is calculated.
5. Update P_0 with P_1 and start over from step 1.

When the sputtered particle collides with Ar, the interaction between the particles is determined by the chosen potential. There are a number of different potentials that may be used, such as the Lennard-Jones potential, the screened Coulomb potential or the hard sphere potential [21]. However, for the relatively low particle energies present here, the choice of the potential does not significantly affect the scattering properties. For simplicity, we chose the less complex hard sphere potential for interactions in the gas phase.

The distance between collisions is determined by the size of the atom. The atomic radius is not a well-defined physical entity and there exist various non-equivalent definitions, e.g. the van der Waals radius, ionic radius, and covalent radius. Alternatively the radius may be empirically measured or calculated from theoretical models. For the simulations we used the calculated atomic radius. This was the most relevant as well as the only type that was accessible for all species involved. The atomic radii for the sputtered elements were defined to be 67 pm for C, 118 pm for Al, 176 pm for Ti, 200 pm for Ta and 71 pm for Ar [22-23]. For the case of two gases, "a" and "b", the mean free path λ_a of "a" in "b" is [24]:

$$\lambda_a = \frac{1}{\sqrt{2}\pi n_a d_a^2 + \sqrt{1+\frac{v_b^2}{v_a^2}} \times n_b \frac{\pi}{4}(d_a + d_b)^2} \quad (1)$$

where *n* is the gas density (m^{-3}), *v* is the mean velocity ($m.s^{-1}$) and *d* is the molecular/atomic diameter (m) for each gas. If "b" denotes the Ar and "a" corresponds to the sputtered atoms, the first term in the denominator can be neglected since the density of the sputtered species is much lower than that of Ar. Further, the value of v_a changes from the velocity corresponding to the initial energy of the sputtered atoms to the thermal equilibrium energy. The latter results in a velocity different from that of Ar, due to mass difference, but it can be assumed to be in the same order of magnitude. By calculating n_b from the ideal gas law and assuming that $\sqrt{1+\frac{v_b^2}{v_a^2}}$ is between 1 and $\sqrt{2}$ it is possible to estimate ranges for the mean free paths of the sputtered atoms. Table 1 summarizes the calculated mean free path for all materials at low and high pressures. In the simulations we have assumed a constant mean free path, corresponding to the one for the thermalized particles, for each combination of material and pressure.

Table 1. *Calculated mean free path (cm) for the sputtered atoms at different sputtering pressures.*

Pressure (Pa)	Mean free path (cm)			
	C	Al	Ti	Ta
0.27	18.4-26.0	9.8-13.8	6.9-9.7	4.8-6.7
2.7	1.8-2.6	1.0-1.4	0.6-0.9	0.5-0.7

4. Results and Discussion

The simulations were carried out in a slightly simplified model of the experimental vacuum chamber. The dimensions were, however, identical. Further, in the experiments there was a dark space shield surrounding the sides of the target extending 0.5 cm from the edge and from the target surface. This shield was omitted in the simulations and consequently the simulations did not account for atoms being deposited onto the shield after being sputtered at high take-off angles (almost parallel to the target surface). Moreover, it was assumed that the target surface was always perfectly flat, in contrast to the experiments, where an erosion area known as a race-track is created. When this occurs, the sputtering angle of the atoms will change relative to the virgin target surface. However, the assumption of a flat target surface is correct in this work since the targets were initially brand new and no significant race-track was observed after the experiments.

The chamber surfaces are divided into a multitude of mesh elements and the number of particles hitting each mesh element is registered. The flux is calculated by dividing the number of incoming particles by the mesh area. By grading the flux in accordance with a colour bar legend, it is possible to visualise the flux distribution over the chamber.

Fig. 2 shows simulation results for the flux distribution of sputtered particles throughout the chamber for each material at low (0.27 Pa) and high (2.7 Pa) pressure. The graphs in Fig. 2 also illustrate a comparison between the experiments and simulations at four different locations in the chamber. The locations are as follows: I – substrate position, II – chamber wall, III – top of the chamber close to the wall and

IV – top of the chamber close to the target. The deposition fluxes in the graphs are normalized to the deposition flux at the substrate (position I). This in order to better illustrate the deposition profile throughout the chamber.

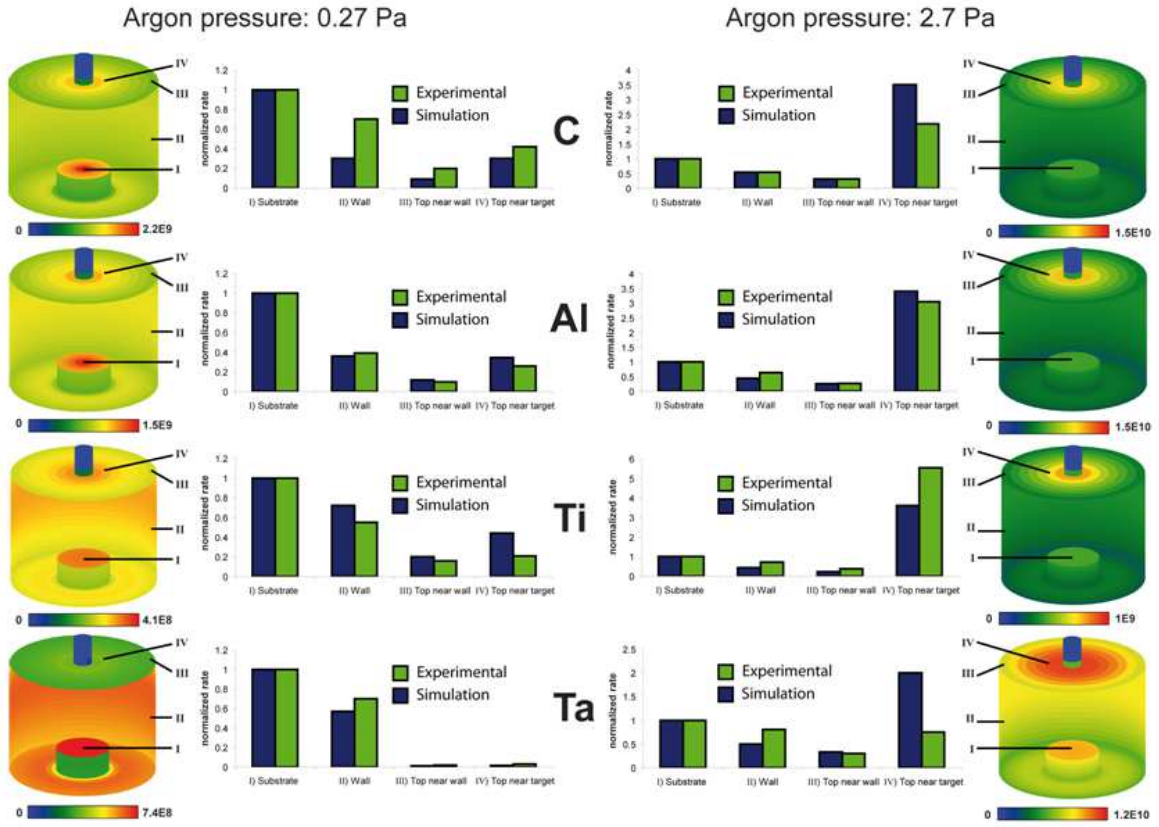

Figure 2. *Simulated flux of sputtered atoms over the chamber at high and low pressures when sputtering from C, Al, Ti and Ta targets. Notice that all colour bar legends have different scales. The graphs show a comparison of experiments and simulations at positions I-IV. The fluxes are normalized to position I for each deposition.*

As a consequence of the normalization procedure, it is not possible to determine the differences between the deposition rates at high and low pressures from Fig. 2. It was, however, concluded from the experiments that the reduction in deposition rate at high pressure compared to low pressure at the substrate (position I) is 27 %, 81 %, 60 % and 73% for C, Al, Ti and Ta respectively.

As expected, a comparison between the deposition rates at positions I and IV reveals significant differences between the elements at low pressure for all materials (Fig. 2). The large Ta atom has a notably smaller mean free path as compared to the smaller C atom, resulting in more frequent collisions. However, the C deposition rate near the target (position IV) is 42% of the rate at the substrate (position I) at low pressure, while it is only 3% for Ta. This means that even though C collides less frequently than Ta, a larger fraction of C atoms is backscattered. The reason for this is the small mass of C, which results in a rather high probability of total reflection after just one collision with Ar. From Table 1 it can be seen that the mean free path of C is estimated to be between 18 cm and 26 cm implying that a significant part of the sputtered C atoms collides with Ar at least one time on its way to the substrate. This is enough to result in a high deposition rate close to the target (position IV). On the other hand, the much heavier and larger Ta is only slightly deflected from its path and more or less continues forward after colliding with Ar. This is especially true during the first few collisions after sputtering when it still has not been thermalized. Several collisions are needed before it can turn around and be backscattered. The higher collision frequency for Ta is not enough to compensate for its smaller average scattering angle. Hardly any atoms will be backscattered, which is illustrated in Fig. 2. C and Ta represent the extreme cases with respect to atomic size and mass. It is therefore expected that the normalized deposition rates of Al and Ti (at position IV, low pressure) fall in between those of C and Ta. The simulated flux of atoms reaching position IV is slightly overestimated due to the absence of dark space shield in the simulations. This enables atoms to be sputtered almost parallel to the target surface (at around 90 degrees). The slightest interaction with Ar could cause a small change of its direction, resulting in a possible hit close to the target. In reality this is prevented from happening by the dark space shield. However, including such a shield in the simulations is a rather complex task and is not motivated by its insignificant impact of the deposition profile elsewhere.

Backscattering is promoted by a low atomic mass

correlated to a small atomic radius, as well as by a high collision frequency correlated to a large atomic radius. The influence of the atomic radius is therefore not straightforward and it may give rise to local minima or maxima in the scattering behaviour. However, such relatively small effects do not change the overall trends and major process behaviours described herein.

At ten times higher pressure (2.7 Pa) the mean free path, being inversely proportional to the pressure, becomes ten times smaller for all materials (Table 1). This implies that all atoms are more or less thermalized when arriving onto the chamber wall or substrate. It is seen that the only material that is quite uniformly deposited all over the chamber is Ta. This is due to the fact that Ta still maintains a portion of its initial direction from the sputtering event due to its high mass, despite its frequent collisions with Ar as it traverses through the chamber.

The other materials are too light to maintain any directionality and their transport through the chamber can be regarded more or less as a diffusion-like process. In such a process the receiving areas closest to the target are exposed to a higher flux of sputtered atoms than areas farther away. For C, Al and Ti, the simulations indicate huge gradients in the flux decreasing rapidly as a function of the distance from the target. A diffusion transport process implies a small mean free path, while the scattering angle distribution should not be significantly biased towards very high or low values. This is mostly valid for Ti, which has a mean free path of around 0.8 cm and a mass that does not predominantly give high or low scattering angles. Al gives similar scattering angles but has a mean free path up to 1.4 cm and is therefore somewhat less diffusion-like. Finally C has an even larger mean free path, up to 2.6 cm, and a scattering angle distribution that is biased towards high scattering angles making it slightly less similar to a diffusion process. The relatively large mean free path of C partially explains the fact that C is the material with the lowest loss in deposition rate (27%) at the substrate (position I) at high pressures. The resemblance to a diffusion process can be estimated by the ratio of the deposition rate close to the target (position IV) and the deposition rate far away from the target (position I). This ratio is highest for Ti, followed by Al, C and Ta. This means that Ti and Al move away from the target in a diffusion-like manner, while the larger mean free path of C and the large mass of Ta make their transport less diffusion-like. This is however only true for this particular combination of processing pressure and chamber dimensions. For a much higher pressure (or larger chamber), the mean free path will be very small compared to the chamber dimensions and subsequently all materials will exhibit a diffusion-like transport.

The different deposition rate distributions for the different elements will inevitably result in compositional gradients in films sputtered from multi-element targets. Such compositional variations have been presented by Neidhardt et. al. who demonstrated substantial compositional variations vs. processing pressure and target to substrate distance in films sputtered from Ti_xB alloy targets [17]. To quantify such gradients, each target was machined into two parts and mounted on the magnetron in different combinations to sputter films of TaC_x, $TaAl_x$, $TaTi_x$ and $TiAl_x$. Since the deposition profile of Ta was significantly different from those of the other materials, Ta was used in combinations with C, Al and Ti to facilitate larger compositional variations over the chamber. This is in contrast to Ti and Al which were combined to promote small compositional variations. Fig. 3 shows simulations of the compositional gradients throughout the chamber for each material combination at low (0.27 Pa) and high (2.7 Pa) pressure. The graphs in Fig. 3 also illustrate a comparison between the experiments and simulations at the same four different locations in the chamber as before.

SRIM was used to define the particle its initial direction and energy as well as sputtering yields. However, the SRIM code contains several artefacts which cause it to over- and under estimate the calculated values of the sputtering yields for heavy and light atoms compared to Ar [25]. Hence, the sputtering yields were taken elsewhere [26]. In the simulations, the sputtering yields were 0.19, 0.78, 0.4 and 0.38 for C, Al, Ti and Ta respectively. These yields change with processing pressures due to a change in target voltage. However, the composition is predominantly determined by the relative sputtering yields which will not be significantly altered. Consequently, if a uniform ion current distribution is assumed over the target, the different target materials combinations correspond to alloy targets of $TaC_{0.5}$, $TaAl_{2.05}$, $TaTi_{1.05}$ and $TiAl_{1.95}$ (these values are referred to as the target composition herein). This means that 0.5 C atoms are sputtered from the Ta/C target for every sputtered Ta (determined by the ratio between the sputtering yields), similar to a $TaC_{0.5}$ alloy target. The major difference is however that the alloy target gives a uniform azimuthal angular distribution of both materials while two target segments put together result in one Ta rich part and one C rich part of the chamber. This is to a large degree compensated by placing the test substrates along the line of symmetry that defines the border between the target halves. The variation in film composition over the chamber is a consequence of the species dependent collision cascades as explained above. As expected, there are huge compositional differences between the top of the chamber and the bottom/wall when Ta is combined with any of the other materials. At low pressures, the concentration of Ta at the chamber top (positions III and IV) is extremely low while the one at the bottom/wall (positions I and II) approaches, and even surpasses, the target composition. The compositional variations are somewhat levelled out at high pressures when more Ta is backscattered to the top of the chamber. This is readily seen in the graphs of Fig. 3 where the white dashed lines correspond to the target compositions. A similar effect was observed by Shaginyan et. al. who demonstrated that sputtering from a WTi (70:30 at%) alloy target resulted in films with dramatically lower W contents at processing pressures below 1 Pa [18]. The compositional

gradients over the chamber are facilitated by the large difference in mass and size between Ta and the other materials. However, the situation is very different when the target is made up of Ti and Al. In this case, the differences in mass and size are less significant and the collision cascades, and consequently the deposition rate distributions, are more similar (see Fig. 2).

This is demonstrated in Fig. 3 which shows much more uniform film compositions over the chamber for both high and low pressures. Moreover, the compositions do not significantly deviate from the target composition.

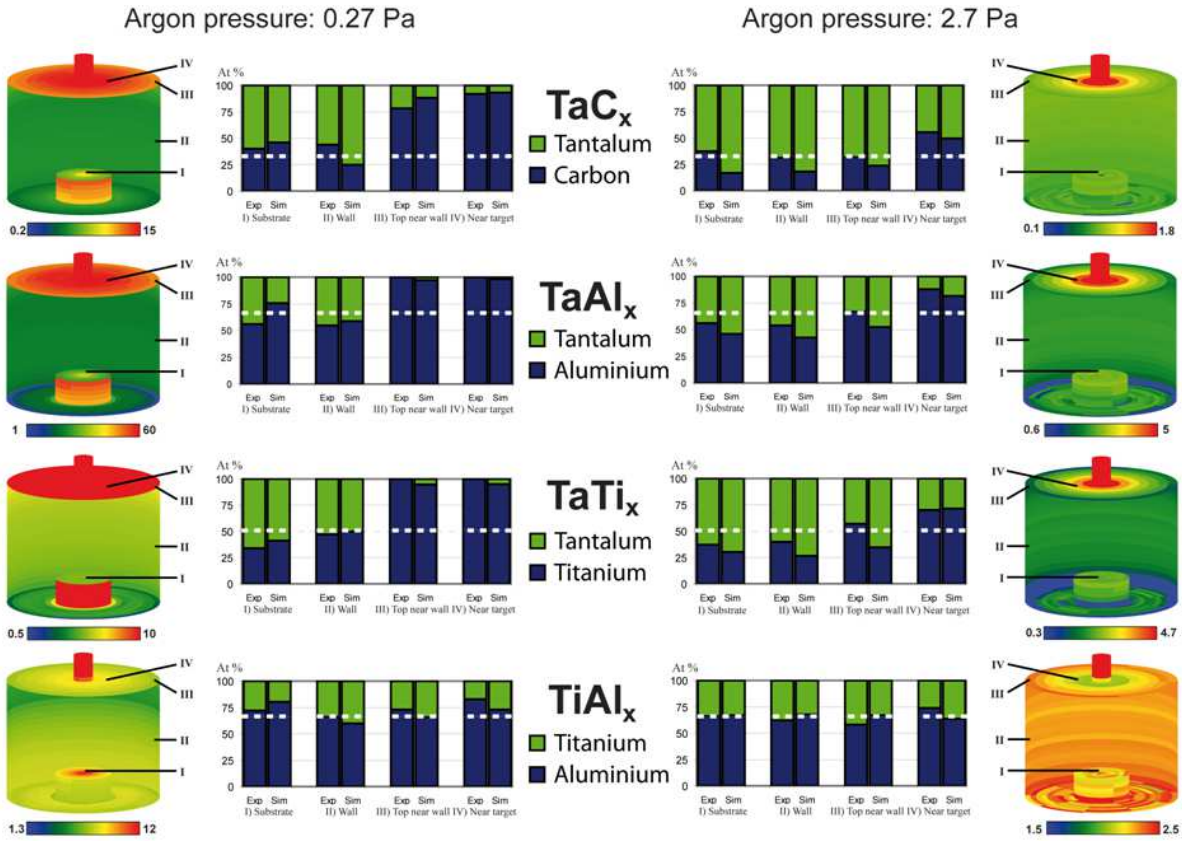

Figure 3. *Simulated film compositions over the chamber at high and low pressures when sputtering from $TaC_{0.5}$, $TaAl_{2.05}$, $TaTi_{1.05}$ and $TiAl_{1.95}$ targets. Notice that all colour bar legends have different scales and represent x in TaC_x, $TaAl_x$, $TaTi_x$ and $TiAl_x$. The graphs show a comparison of experiments and simulations at positions I-IV. The white dashed line in the graphs corresponds to the target compositions.*

It should be pointed out that there may be effects that could take place under certain conditions that can influence the film composition and that are not accounted for here. Fore instance, there may be backscattered Ar atoms, which could preferentially sputter the growing film. However, this may only occur at low pressure since reflected Ar atoms will be effectively thermalized at higher pressures. In the case of sputtering from e.g. an oxide or WS_2 target, there will also be negative oxygen or sulphur ions, accelerated by the target potential towards the growing film causing preferential sputtering. Further, the different atoms may have different sticking coefficients. In the simulations here, all atoms arriving at the wall or substrate are assumed to have a sticking probability of 1.

5. Summary and Conclusions

This work investigates both experimentally as well as by simulations the deposition rate distribution from four elemental targets (C, Al, Ti and Ta) as well as the compositional gradients from four multi-element targets (Ta/C, Ta/Al, Ta/Ti and Ti/Al) sputtered at two relatively extreme process pressures. At relatively low pressures (0.27 Pa), it is shown that a substantial amount of C, Al and Ti atoms are backscattered. This leads to deposition rates near the target ranging from 20% to 45% of those obtained at the substrate position. However, the significantly heavier and larger Ta atoms are less affected by interactions with Ar atoms at this low pressure and a negligible amount is backscattered. C is very light and small and is therefore backscattered to a large extent even though its small size implies a long mean free path. The higher atomic masses of Al and Ti reduce the probability of large angle deflection in a single collision. However, this is compensated by a larger atomic radius resulting in higher collision frequencies. The much larger Ta atom collides even more frequently but due to its high mass, its direction is only slightly changed in each collision.

At ten times higher pressure (2.7 Pa), the mean free path is ten times smaller. Here the collision frequency is so high that

all atoms, regardless of mass, become thermalized before arriving at the substrate/chamber wall. This results in 2-5 times higher deposition rates close to the target as compared to those at the substrate for C, Al and Ti targets. For these materials, the transport of sputtered atoms away from the target can be roughly approximated with a diffusion process. However, Ta is heavy enough to maintain a certain directionality towards the substrate and the experimental deposition rate close to the target is of the same order as the one at the substrate.

Both simulations and experiments are in agreement and show a significant influence from the processing pressure as well as the mass of the sputtered atoms on the deposition rate throughout the chamber. The amount of backscattered material is significant for C, Al and Ti even at low pressures. A more efficient process, where less material is wasted, may be obtained if the process is operated at lower pressure or if the dimensions, especially the target-to-substrate distance, is reduced. The effect of such process optimization is species dependent and may be non-linear, meaning that a very small reduction of the pressure or distance may result in a substantially more efficient process.

The element specific flux distributions give rise to compositional gradients in films sputtered from multi-elemental targets. Targets made from Ta/C, Ta/Al, Ta/Ti resulted in significant gradients over the chamber at a low pressure and slightly smaller gradients at higher pressure. The main reasons for the gradients are the large size and heavy mass of Ta, causing it to traverse differently from the smaller and lighter atoms. However, targets made from Ti/Al resulted in a more uniform composition (close to the target composition) over the chamber for both high and low pressures. Since the mass and size of these atoms are not very different, their trajectories are not that different and consequently the gradients are smaller and the film compositions are closer to that of the target. It can be concluded that it is easier to obtain film compositions equal to the target by keeping the distance between the target and substrate as low as possible to minimize the scattering with argon. This is however only required if the target is made of constituents far away from each other in the periodic system, i.e. they have a large difference in mass and size.

The results presented here may be used as guidelines to design experiments to predict the deposition profiles for arbitrary materials and variation of film compositions for any combination of target materials at different processing pressures. This is useful when estimating the uniformity (with respect to thickness and/or composition) over large or non-flat substrates as well as minimizing the material loss inside the chamber.

Acknowledgements

The authors gratefully acknowledge the Swedish Foundation for Strategic Research for financial support through the project *Technical advancement through controlled tribofilms.*

References

[1] DT. Motohiro and Y. Taga, “Monte Carlo simulation of the particle transport process in sputter deposition,” Thin Solid Films 112, 161 (1984).

[2] C. Vitelaru, L. de Poucques, T. M. Minea, and G. Popa, “Space-resolved velocity and flux distributions of sputtered Ti atoms in a planar circular magnetron discharge,” Plasma Sources Sci. Technol. 20, 045020 (2011).

[3] F. Boydens, W. P. Leroy, R. Persoons, and D. Depla, “The influence of target surface morphology on the deposition flux during direct-current magnetron sputtering,” Thin Solid Films 531, 32 (2013).

[4] K. Macàk, P. Macàk, and U. Helmersson, “Monte Carlo simulations of the transport of sputtered particles,” Computer Physics Communications 120, 238 (1999).

[5] A. Malaurie and A. Bessaudou, “Numerical simulation of the characteristics of the different metallic species falling on the growing film in d.c. magnetron sputtering,” Thin Solid Films 286, 305 (1996).

[6] P. K. Petrov, V. A. Volpyas, and R. A. Chakalov, “Three-dimensional Monte Carlo simulation of sputtered atom transport in the process of ion-plasma sputter deposition of multicomponent thin film,” Vacuum 52, 427 (1999).

[7] J. Stache, “Hybrid modeling of deposition profiles in magnetron sputtering systems,” J. Vac. Sci. technol. A 12, 2867 (1994).

[8] T. Nakano and S. Baba, “Gas pressure effects on thickness uniformity and circumvented deposition during sputter deposition process,” Vacuum 80, 647 (2006).

[9] G. Yamamura and N. Ishida, “Monte Carlo simulation of the thermalization of sputtered atoms and reflected atoms in the magnetron sputtering discharge,” J. Vac. Sci. Technol. A 13, 101 (1995).

[10] G. M. Turner, I. S. Falconer, B. W. James, and D. R. McKenzie, “Monte Carlo calculations of the properties of sputtered atoms at a substrate surface in a magnetron discharge,” J. Vac. Sci. Technol. A 10, 455 (1992).

[11] M. Horkel, K. Van Aeken, C. Eisenmenger-Sittner, D. Depla, S. Mahieu, and W.P. Leroy, “Experimental determination and simulation of the angular distribution of the metal flux during magnetron sputter deposition,” J. Phys. D: Appl. Phys. 43, 075302 (2010).

[12] W. D. Westwood, “Calculation of deposition rates in diode sputtering systems,” J. Vac. Sci. Technol., 15, 1 (1978).

[13] A. M. Myers, J. R. Doyle, J. R. Abelson, and D. N. Ruzic, “Monte Carlo simulations of magnetron sputtering particle transport,” J. Vac. Sci. Technol. A 9, 614 (1991).

[14] K. Van Haeken, S. Mahieu, and D. Depla, “The metal flux from a rotating cylindrical magnetron: a Monte Carlo simulation,” J. Phys. D: Appl. Phys. 41, 205307 (2008).

[15] T. Yagisawa and T. Makabe, “Modeling of dc magnetron plasma for sputtering: Transport of sputtered copper atoms,” J. Vac. Sci. Technol. A 24, 908 (2006).

[16] S. Mahieu, G. Buyle, D. Depla, S. Heirwegh, P. Ghekiere, and R. De Gryse, "Monte Carlo simulation of the transport of atoms in DC magnetron sputtering," Nucl. Instrum. Methods Phys. Res. B 243, 313 (2006).

[17] J. Neidhardt, et. al., "Experiment and simulation of the compositional evolution of TiB thin films deposited by sputtering of a compound target," Journal of applied physics, 104, (2008).

[18] L. R. Shaginyan, M. Mišina, S. Kadlec, L. Jastrabk, A. Macková, and V. Peina, "Mechanism of the film composition formation during magnetron sputtering of WTi," J. Vac. Sci. Technol. A 19, 2554 (2001)

[19] S. B. Krupanidhi and M. Sayer, "Position and pressure in rf magnetron reactive sputter deposition of piezoelectric zinc oxide," J. Appl. Phys. 56, 3308 (1984).

[20] J. F. Ziegler, J. Biersack, M. D. Littmark, "The Stopping and Range of Ions in Matter," New York: Pergamon Press (1985). ISSN 0891-5490.

[21] W. Eckstein, "Computer Simulation of Ion-Solid Interactions," Springer-Verlag, Volume 10, 1991, ISBN 978-3-642-73515-8

[22] E. Clementi, D. L. Raimondi, and W. P. Reinhardt, "Atomic screening constants from SCF functions. II. Atoms with 37 to 86 electrons," J. Chem. Phys. 47, 1300 (1967).

[23] E. Clementi and D. L. Raimondi, "Atomic screening constants from SCF functions," J. Chem. Phys. 38, 2686 (1963).

[24] J. F. O'Hanlon, "A user's guide to vacuum technology," John Wiley & Sons, Inc., Hoboken, New Jersey, 2003). ISBN 0-471-81242-0

[25] K. Wittmaack, "Reliability of a popular simulation code for predicting sputtering yields of solids and range of low-energy ions," J. Appl. Phys. 96, 2632 (2004).

[26] N. Matsunami, Y. Yamamura, Y. Itikawa, N. Itoh, Y. Kazumata, S. Miyagawa, K. Morita, R. Shimizu, H. Tawara, "Energy dependence of the ion-induced sputtering yields of monoatomic solids," Atomic Data and Nuclear Data Tables, v.31, p.1-80 (1984).